

KNOTS IN BISTABLE REACTING SYSTEMS

ANATOLY MALEVANETS

*Department of Physics, Theoretical Physics, 1 Keble Road,
Oxford OX1 3NP, England*

RAYMOND KAPRAL

*Chemical Physics Theory Group, Department of Chemistry,
University of Toronto, Toronto M5S 3H6 Canada*

Bistable chemically reacting media can segregate into domains of two stable phases that differ in their chemical composition and are separated by chemical fronts. For activator-inhibitor kinetics, when the diffusion coefficient of the inhibitor is greater than that of the activator, stable localized chemical patterns can form. These localized structures arise from the interaction between chemical fronts as a consequence of the fast inhibitor diffusion. In three dimensions one can build linked and knotted chemical dissipative structures whose stability is a consequence of their topology. In the general case, the evolution equations that govern the pattern formation are not of gradient type but the stable chemical patterns assume nearly ideal forms.

1 Introduction

Open chemically reacting systems forced out of equilibrium by flows of reagents may evolve to patterned stationary or time-dependent states.¹ We shall be concerned with bistable reacting media where the system may evolve to either of two stable states that differ in their chemical compositions. In a spatially-distributed system these two stable states may exist in different regions of space separated by interfaces across which the chemical concentrations change sharply, akin to a mixture of oil in water. In three dimensions a tubular domain containing one of the stable phases may have the topology of a link or knot embedded in a “sea” of the other stable phase.^{2,3} These compact stable structures rely on their topology for their existence: in the absence of a linked or knotted geometry the tubular domains that comprise these structures shrink to balls. Such compact stable structures are termed topologically stabilized patterns.

These topologically stabilized patterns are seen in multi-component reaction-diffusion systems which, in general, are not of gradient form: the patterns are dissipative structures. It is then interesting to consider the factors that determine the final geometries of the linked and knotted patterns. We shall show that the links and knots are approximately ideal⁴ and this fact can be ascribed to the interactions that are responsible for their existence.

Section 2 describes the FitzHugh-Nagumo (FHN) reaction-diffusion system used to illustrate the formation of topologically stabilized patterns. This model, which has its origins in nerve impulse propagation, is believed to capture the essential features of real bistable media which support localized localized chemical patterns, the antecedents of the knotted topologies discussed here. Our simulations are actually carried out on a microscopic reaction model whose mean field limit is the FitzHugh-Nagumo equation. We describe the construction of the stochastic model in Sec. 3. As a result, the chemical patterns we find arise from the random reactive and diffusive motion of millions of particles and their existence demonstrates the robustness of the chemical patterns to molecular fluctuations. The localized linked and knotted patterns are analyzed in Sec. 4 on the basis of their ideal structures, while the conclusions of this study are given in Sec. 5.

2 Competing Interactions in Bistable Media

The chemical patterns we shall describe arise from competing activator-inhibitor kinetics. The FitzHugh-Nagumo reaction-diffusion equation,^{5,6}

$$\begin{aligned}\frac{\partial u}{\partial t} &= -u^3 + u - v + D_u \nabla^2 u, \\ \frac{\partial v}{\partial t} &= \epsilon(u - \alpha v - \beta) + D_v \nabla^2 v,\end{aligned}\tag{1}$$

is such an activator-inhibitor system. An increase in the concentration of the activator u leads to an increase in its own production and that of v ; an increase in the concentration of the inhibitor v suppresses the production of chemical species. The interplay between these two “species” is responsible for the effects we shall describe.

For the moment suppose the system is spatially homogeneous and the diffusion terms in Eq. (1) are absent. The u and v nullclines of the resulting ordinary differential equation, the equations for $\dot{u} = 0$ and $\dot{v} = 0$, are shown in Fig. 1. As drawn, there are three intersections between the u and v nullclines. Linear stability analysis shows that the outer two fixed points are stable while the central fixed point is unstable. This is the bistable regime discussed above: depending on the initial values of u and v , the system will evolve to either of these two stable fixed points.

Next, suppose we reintroduce the diffusion terms and consider a spatially-distributed system described by Eq. (1). Inhomogeneous initial states will evolve to form domains of the two stable phases. The structure and dynamics of these domains, which depend on the interplay between the activator-inhibitor

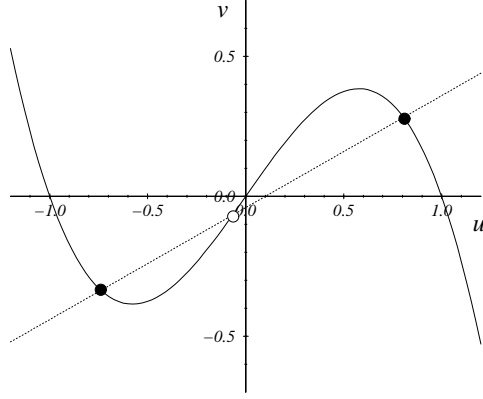


Figure 1: Nullclines of the FitzHugh-Nagumo equation for parameters in the bistable regime. The linear v nullcline intersects the cubic u nullcline in three fixed points; the outer two denoted by filled circles are stable while the central fixed point denoted by an open circle is unstable.

kinetics and the relative values of the diffusion coefficients of these species, are the topics of this chapter.

The FHN reaction-diffusion equation is not of gradient form and there is no free energy functional that controls the evolution to the final attracting states. In order to examine the structure of Eq. (1) it is convenient to formally solve the linear equation for the inhibitor v and write the equation for the activator u as,

$$\frac{\partial u(\mathbf{r}, t)}{\partial t} = -u^3 + u + D_u \nabla^2 u - \int_V d\mathbf{r}' \int dt' G(\mathbf{r} - \mathbf{r}', t - t') \epsilon(u(\mathbf{r}', t') - \beta), \quad (2)$$

where the Green function $G(\mathbf{r}, t)$ is given by

$$G(\mathbf{r}, t) = (4\pi D_v t)^{-3/2} e^{-\alpha \epsilon t - r^2/4D_v t}. \quad (3)$$

From this form we can see that the activator field at space-time point (\mathbf{r}, t) is influenced by its value at point (\mathbf{r}', t') due to coupling with the inhibitor field. In this general form the evolution equation cannot be written as the gradient of a free energy functional. However, if ϵ is large so that v varies on a much

faster time scale than that of u , we may let $u(\mathbf{r}', t') \approx u(\mathbf{r}', t)$ in the integral in Eq. (2) and, after integration, obtain,

$$\frac{\partial u(\mathbf{r}, t)}{\partial t} = -u^3 + u + \frac{\beta}{\alpha} + D_u \nabla^2 u - \int_V d\mathbf{r}' G(\mathbf{r}) u(\mathbf{r}', t), \quad (4)$$

with

$$G(\mathbf{r}) = (4\pi \tilde{D}_v r)^{-1} e^{-\kappa r}. \quad (5)$$

Here $\kappa = (\alpha/\tilde{D}_v)^{1/2}$ and the scaled diffusion coefficient of the activator is $\tilde{D}_v = D_v/\epsilon$. Now Eq. (4) can be written in gradient form

$$\frac{\partial u(\mathbf{r}, t)}{\partial t} = -\frac{\delta \mathcal{F}}{\delta u}, \quad (6)$$

where the nonlocal free energy functional \mathcal{F} is

$$\mathcal{F} = \int d\mathbf{r} \left(\mathcal{V}(u) + \frac{D_u}{2} |\nabla u|^2 \right) + \frac{1}{2} \int d\mathbf{r} \int d\mathbf{r}' u(\mathbf{r}) G(\mathbf{r} - \mathbf{r}') u(\mathbf{r}'). \quad (7)$$

The potential \mathcal{V} is defined as $\mathcal{V}(u) = u^4/4 - u^2/2 - \beta u/\alpha$. With these results in hand we may review some of the features of this type of activator-inhibitor kinetics. First, we note that if the scaled diffusion coefficient of the inhibitor tends to zero, Eq. (4) reduces to the time-dependent Ginzburg-Landau equation (model A for a non-conserved order parameter of critical phenomena⁷). It is well known that this equation exhibits domain coarsening: if the system is prepared in the unstable state domains of the two stable phases will form and grow. The growth law and the nature of the domains depends on whether the potential \mathcal{V} is symmetric or asymmetric. For an asymmetric free energy potential with $\beta \neq 0$, if two phases are separated by a planar interface, the more-stable phase will consume the less-stable phase at a rate determined by the planar front velocity. For more complicated phase geometries the front velocity and domain curvature determine the coarsening rate.⁸

The situation changes if $D_v \gg D_u$. As indicated above in the fast inhibitor limit the additional long-range term in the free energy functional gives rise to a competing interaction that leads to the possibility of modulated phases or localized patterns. These localized patterns are observed both in the fast inhibitor limit (Eq. (4) and in the general case or slow inhibitor limit (Eq. (2)).⁹⁻¹⁴ When the inhibitor diffuses rapidly compared to the activator, the long-ranged v field influences the interactions among the u -field fronts, leading to front repulsion in certain parameter regimes. Such front repulsion can give rise to isolated structures of the less-stable phase in a sea of the more stable phase.^{9,10} In

the absence of such front repulsion the small domains of the less-stable phase would be consumed by the more-stable phase.

We also note that for a different model with a nonlocal energy functional it was demonstrated^{15,16} that compact stable patterns exist. The stable patterns are defined by the local minima of the functional and their form is defined by the tendency of the system to maximize surface contact area at a fixed distance and minimize the volume of the minority state. These structures are closely related to the two dimensional patterns that exist in the FHN system in the large ϵ limit^{11,12} and their shape can take rather complicated forms.

We shall be concerned with the limit where the inhibitor diffuses rapidly compared to the activator and localized structures are possible. The basic building block for the three-dimensional chemical patterns discussed here is a tubular domain of the less-stable phase in a “sea” of the more-stable phase. Depending on the system parameters, such tubular domains may either grow, with fingering instabilities in some parameter ranges or shrink to balls as shown in Fig. 2.³ Recall that because chemical reactions can change the numbers of

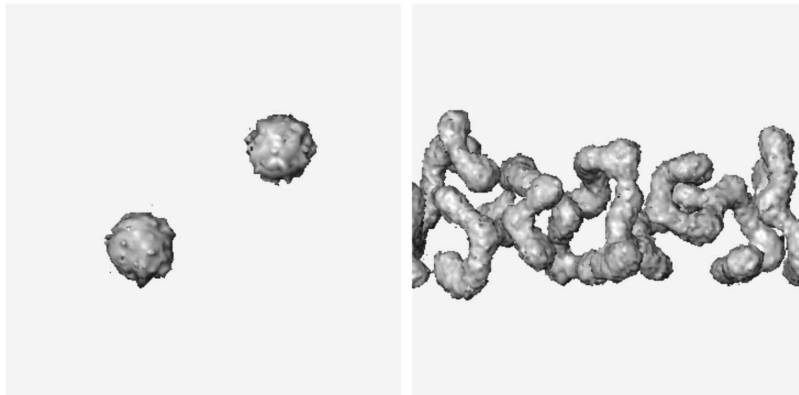


Figure 2: Contraction of a tubular domain to a ball (left panel); growth of a tubular domain by fingering instabilities (right panel). System parameters are: $\alpha = 5.2$, $\beta = 0.33$, $\epsilon = 0.0055$ and $\alpha = 5.4$, $\beta = 0$, $\epsilon = 0.0085$, respectively. The diffusion ratio is $D_b/D_a = 4$.

chemical species we have non-conserved dynamics and the amount of a given phase is not fixed by the initial preparation of the system.

Before presenting a discussion how the above considerations lead to the possibility of stable linked and knotted patterns, we give an account of the stochastic dynamics that is actually used to simulate the chemical patterns. The use of a stochastic model, rather than the FHN reaction-diffusion equation,

not only allows us to probe the mesoscale origin of chemical pattern formation, but also demonstrates that the chemical patterns we find are robust to molecular fluctuations.

3 Stochastic Model

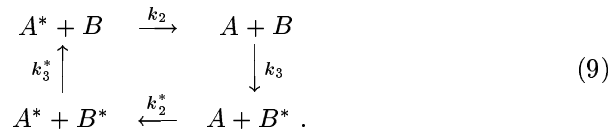
Microscopic Markov chain models utilize stochastic rules that simulate both the reactive collision events that are responsible for the interconversion of chemical species and the random walk dynamics that lead to diffusive transport in the medium. The u and v variables in the FHN model do not directly correspond to the concentrations of chemical species, nor is a chemical mechanism usually associated with this kinetic equation.

In order to formulate a microscopically-based stochastic model it is first necessary to provide a mechanism whose mass action law is the FHN kinetic equation. Some features of the FHN kinetics seem to preclude such a mechanistic description; for instance, the production of u is inhibited by a term linear in v , a contribution not usually encountered in mass action kinetics. However, if each local region of space is assumed to be able to accommodate only a maximum number N of each chemical species, then such a mechanism may be written.^{2,3} We assume that the chemical reactions depend on the local number of molecules of the species as well as the number of vacancies corresponding to each species, in analogy with the dependence of some surface reactions on the number of vacant surface sites or biochemical reactions involving complexes of allosteric enzymes that depend on the number of vacant active sites.

The reaction mechanism consists of the cubic autocatalytic steps involving species A and its corresponding vacancy species A^* ,



This part of the mechanism is responsible for the bistability of the system but, in the absence of other coupling, will simply give rise to stable states corresponding to full occupancy or complete vacancy at a site. A second species B involved in bimolecular reactions with A is needed to account for both the linear and cubic parts of the FHN model. The following cyclic reaction steps accomplish this:



Many mechanisms may give rise to the same chemical rate law and this mechanism may be considered as the definition of the microscopic reactive dynamics. Assuming mass action kinetics, we may write the following chemical rate law from a knowledge of this mechanism:

$$\begin{aligned}\frac{da}{dt} &= \{k_1 a - k_1^*(1-a)\}a(1-a) + k_2(1-a)b - k_2^*a(1-b), \\ \frac{db}{dt} &= k_3^*(1-a)(1-b) - k_3 ab,\end{aligned}\tag{10}$$

where a and b are the average fractional occupancies of a site. For $k_2^* = k_2$ and $k_3^* = k_3$, these equations can be converted to FHN form with the linear change of variables, $a = c_a u + a_0$ and $b = c_b v + b_0$ where

$$\begin{aligned}c_a^2 &= \frac{1}{3} \left(\frac{k_1 + 2k_1^*}{k_1 + k_1^*} \right)^2 - \frac{k_2 + k_1^*}{k_1 + k_1^*}, a_0 = \frac{1}{3} \frac{k_1 + 2k_1^*}{k_1 + k_1^*}, \\ c_b &= -\frac{k_1 + k_1^*}{k_2} c_a^3, b_0 = a_0 \frac{c_b}{c_a} \left\{ 1 - \left(\frac{a_0}{c_a} \right)^2 \right\},\end{aligned}\tag{11}$$

and use of the scaled time variable $\tau = t/\tau_s$ with $\tau_s^{-1} = (k_1 + k_1^*)c_a^2$. The parameters in (1) are related to the rate constants by

$$\alpha = -\frac{c_b}{c_a}, \quad \beta = \frac{1 - a_0 - b_0}{c_a}, \quad \epsilon = \frac{k_3}{k_2} \left(\frac{c_a}{c_b} \right)^2.\tag{12}$$

Using these relations one may choose desired values of the FHN parameters α , β and ϵ by tuning the values of the rate constants in the mechanism. In this way we can select parameter domains that are likely to favor isolated domain structures where linked and knotted patterns are expected to be found.

To construct a Markov chain model we suppose the dynamics takes place on a regular lattice and that the local spatial regions are associated with sites on this lattice. The Markov chain model then requires that transition probabilities be defined for the local reactive transformations at a lattice site and for the hops from a given site to neighboring sites in order to simulate the random walks that lead to diffusive motion of the species. Here we give a brief account of the strategy used to build the stochastic model and its relation to the mass action rate law. In the Appendix we give a more detailed analysis of the Markov chain to show how the reaction-diffusion equation can be obtained.

Once a reaction mechanism has been specified, the reaction transition probabilities are easily constructed by implementing birth-death stochastic rules¹⁷ for the reactions. At each time step one of the six reactions in the

mechanism (labeled by the index j) is chosen at random and takes place with a probability given by

$$p_j = \gamma \bar{k}_j N \prod_{\kappa=A}^B \frac{n_\kappa!}{(n_\kappa - \nu_\kappa^{(j)})!} \frac{n_\kappa^*!}{(n_\kappa^* - \nu_\kappa^{*(j)})!} \frac{(N - \nu_\kappa^{(j)} - \nu_\kappa^{*(j)})!}{N!}, \quad (13)$$

where $n_\kappa^* = N - n_\kappa$, $\nu_\kappa^{(j)}$ and $\nu_\kappa^{*(j)}$ are the stoichiometric coefficients for species κ and κ^* , respectively, in reaction j and $\bar{k}_{2i-1} = k_i$ and $\bar{k}_{2i} = k_i^*$ for $i = 1, 2, 3$. Here γ is a constant that determines the overall time scale of the reactive transformations. These reaction probabilities simply state that the probability of a given reaction step is proportional to the macroscopic rate constant for that step, times the number of possible ways that reaction can occur for the given numbers of A and B molecules at the site.

To simulate diffusion, random walk transition probabilities are chosen so that the probability of a hop to a neighboring node $p(n_\kappa)$ is linear in the fractional occupancy of the site and $p(0) = 0$ and $p(N) = 1$ to insure that the the occupation number never falls below zero or is greater than N (exclusion principle is always satisfied).^{2,3} This choice of transition probabilities guarantees that the diffusion coefficient is independent of n_κ . One may show that this diffusion rule leads to a binomial stationary distribution (cf. Appendix),

$$p_{n_A}^B = \binom{N}{n_A} a^{n_A} (1-a)^{N-n_A}, \quad (14)$$

with a similar equation for species B . If diffusion can maintain the a local binomial distribution during the course of slow reactive interconversions between A and B species, the time rate of change of of the average particle densities due to reactions is given by

$$\frac{d\bar{n}_\kappa}{dt} = \sum_{j=1}^6 \sum_{n_A, n_B} (\Delta n_\kappa)_j p_j p_{n_A}^B p_{n_B}^B, \quad (15)$$

where $(\Delta n_\kappa)_j$ is the change in particle number of species κ in the j th reaction. Direct evaluation of the r.h.s. of this equation leads to the mass action law Eq. (10). This confirms that the Markov chain model yields the mass action law in the limit of perfect diffusive mixing.

In the Appendix we show that the reaction-diffusion equation, Eq. (1), is obtained in the limit of slow reaction and small spatial gradients. Consequently, we may use the Markov chain model in suitable parameter regimes to simulate the reaction-diffusion system (this is the limit with which we shall be primarily be concerned in this chapter) or investigate the breakdown of such macroscopic models due to reactive correlations.²

3.1 Simulation details

In the simulations reported in this chapter the random walk dynamics is realized by use of an auxiliary “excited” particle lattice. At each step at most one particle per site is transferred to the excited state with a probability depending on the site occupation number as described above. Next, the excited particles are translated one lattice unit in a random direction chosen from a set $V = \{\mathbf{v}_1, \dots, \mathbf{v}_k\}$. Finally, the excited particles are placed in new lattice positions. For the three-dimensional simulations, rather than using the simple cubic lattice, we have taken the set V to represent the projections of the normals of the four-dimensional FCC Wigner-Seitz cell on the three-dimensional space.¹⁸ The diffusion rule leads to mixing of particles on the lattice and, to a good approximation, it establishes a local binomial probability distribution of particle numbers.² The use of a 24-direction diffusion rule is motivated by symmetry considerations. The FCC set of directions given by the six permutations of $(\pm 1, \pm 1, 0, 0)$ leads to a spherically symmetric discrete Laplacian with fourth-order corrections in the lattice spacing.

The kinetic and diffusion parameters were the same for all simulations with the exception of the growing patterns in Fig. 2 (right panel) whose parameters are given in the caption. The parameters were selected to be: $\tilde{k}_1 = 0.862$, $\tilde{k}_1^* = 0.76$, $\tilde{k}_2 = 0.04$ and $\tilde{k}_3 = 0.006$. The maximum occupancy per node was taken to be $N = 7$ and the diffusion coefficient ratio was $D_b/D_a = 4$. The kinetic parameters correspond to the following FHN parameters: $\alpha = 5.21$, $\beta = 0.33$ and $\epsilon = 0.0055$. The calculations were performed on $256 \times 256 \times 256$ lattices for the Borromean rings and 4_1 knot, on $256 \times 256 \times 128$ lattices for the 3_1 knot and on $256 \times 128 \times 128$ lattices for the Hopf link. The simulations were carried out on a CAM-8 machine¹⁹ that is designed for lattice-gas models of the type used here.

4 Links and Knots

In this section we show how the domain dynamics and existence of localized structures described earlier can lead to stable links and knots. We consider the regime where tubular domains shrink. A tubular domain shrinks by contracting at its free ends, maintaining a fixed diameter until the final stages of the contraction where a ball is formed as in Fig. 2. Suppose that the tubular domain has no free ends but is instead a completely connected domain in three-dimensional space. Now the entire continuous tubular domain will contract with diffusion providing an effective mean force that tends to reduce the curvature. Such contraction may again yield a ball but it is possible that the

local repulsion between fronts that arises from the rapidly diffusing inhibitor species will be sufficiently strong that collapse is prevented and a stable compact structure results which retains the linked or knotted topology of the initial condition.^a That this is indeed the case is demonstrated by the Hopf and Borromean links and 3_1 and 4_1 knots shown in Figs. 3 and 4. In these figures

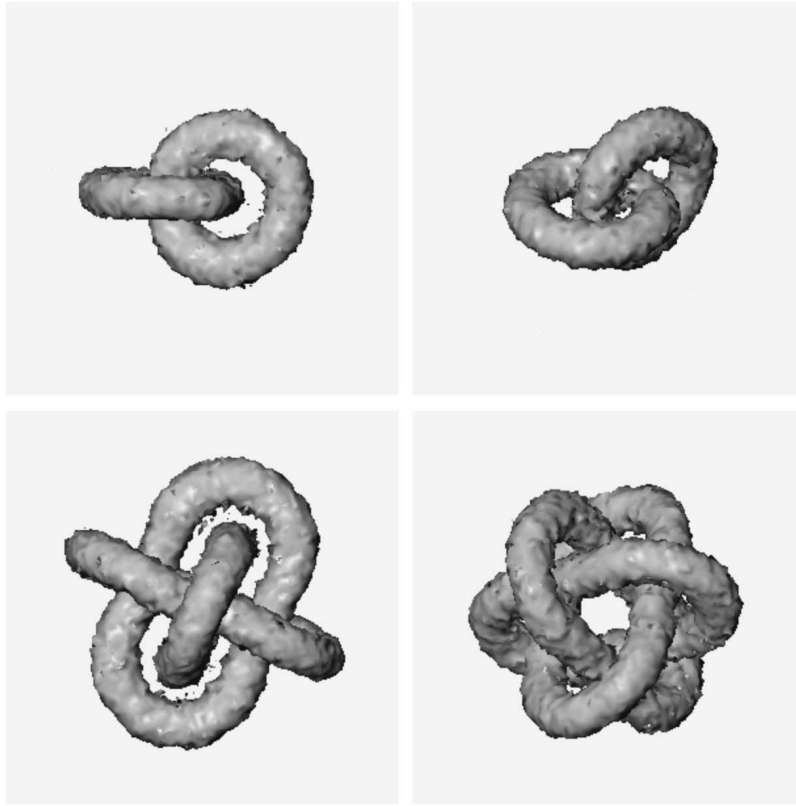


Figure 3: Hopf (800K time steps) and Borromean ($> 1M$ time steps) links. Two different views are shown for each link.

isoconcentration surfaces corresponding to the activator are shown. The imperfections in these surfaces are due primarily to the fact that the dynamics is

^aThe stable localized three-dimensional patterns described in Refs.^{16, 15} are akin to the stable ball-like configurations in Fig. 2 and are not topologically stabilized like the structures considered in this chapter.

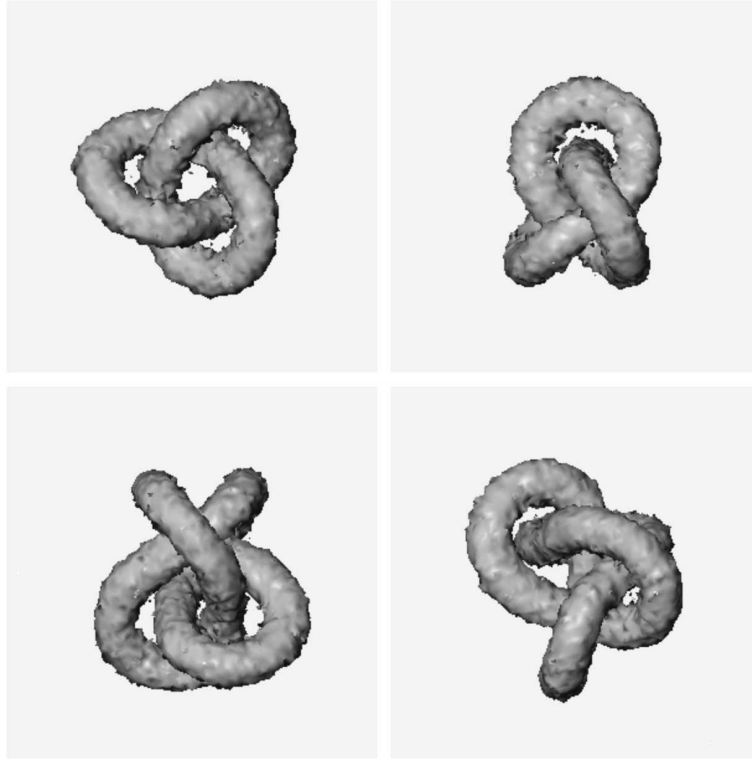


Figure 4: 3_1 (2.6M time steps) and 4_1 (4M time steps) knots. Two different views are shown for each knot.

stochastic and the concentration fields are determined by coarse graining the particle numbers in local spatial regions; hence, molecular fluctuations exist and their effects can be seen in these figures. Molecular fluctuations have another consequence: none of these patterns is truly stable but rather metastable since fluctuations can occasionally lead to breaking of a tubular domain. This fluctuation effect can be controlled by changing the spatial scale by tuning the diffusion relative to reaction. The parameters in our simulations are such that fluctuation effects are almost negligible and the simulation results approximate those of the FHN reaction-diffusion equation. We have never observed fluctuation breaking of the Borromean rings or 3_1 or 4_1 knots on the time scale of our simulations; we have observed breaking of the Hopf link for sufficiently long times for some realizations of the stochastic evolution.

Plots of the local curvature and torsion provide quantitative information about the geometrical structure of the patterns. The curvature $\kappa(\sigma)$ is defined as,²⁰

$$\kappa = \frac{|\mathbf{R}_\sigma \times \mathbf{R}_{\sigma\sigma}|}{|\mathbf{R}_\sigma|^3}. \quad (16)$$

To compute this quantity the curve $\mathbf{R}(\sigma)$ was extracted from an analysis of the concentration fields of the links and knots. This curve was constructed so that the parameterization of the line σ was approximately proportional to the natural parameterization s . Equation (16) is invariant with respect to the change of variable $\sigma = \sigma(s)$. The curvatures of the 3_1 and 4_1 knots are shown in Fig. 5. From this figure one can see that the 3_1 knot has the expected three-

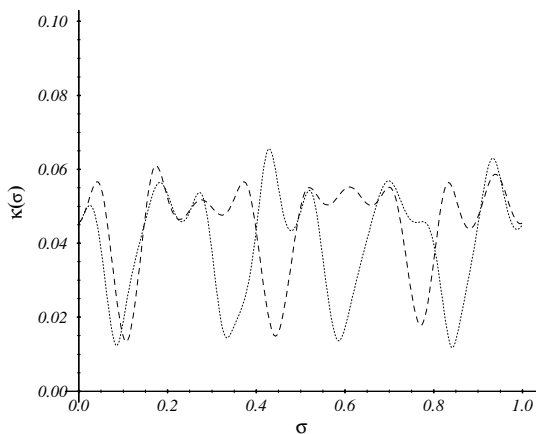


Figure 5: Local curvatures as a function of σ for the 3_1 knot (dashed line) and the 4_1 knot (solid line).

fold symmetry to a good approximation. Its curvature is nearly constant at a value of around $\kappa = 0.05$ except for three region of σ where it assumes small values. In these regions the tubular domain passes through a knot loop and the tube has a nearly linear segment. More significant variations of the curvature with σ are seen for the 4_1 knot. Its more complex form leads to additional regions where a tubular domain must pass through a knot loop leading to stronger variations in the curvature.

An examination of the local torsion, $\tau(\sigma)$, defined by

$$\tau = \frac{(\mathbf{R}_\sigma \times \mathbf{R}_{\sigma\sigma}) \cdot \mathbf{R}_{\sigma\sigma\sigma}}{|\mathbf{R}_\sigma \times \mathbf{R}_{\sigma\sigma}|^2}, \quad (17)$$

provides information on the planarity of the structures. The local torsion is shown in Fig. 6. One can see large segments of σ where the torsion is near

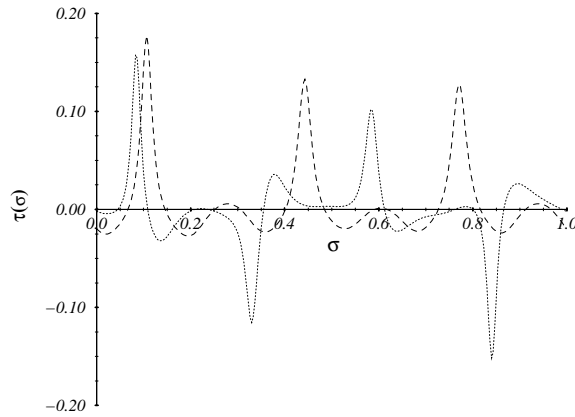


Figure 6: Local torsion as a function of σ of the 3_1 (dashed line) and 4_1 (solid line) knots.

zero for both knots, indicating planarity. The 3_1 knot is built from three such planar regions as expected (one can see some deviation from perfect symmetry likely due to transient effects in the relaxation to the final stable knot), while the 4_1 knot is built from four such planar regions with smaller extent.

4.1 Ideal links and knots

It is difficult to predict the final stable forms of the links and knots in the bistable reacting medium. As discussed above, in general there is no free energy functional whose minimization yields the stable structures. The main feature that is responsible for the formation of these chemical patterns is the front repulsion that arises through the mediation of the fast diffusion of the inhibitor field. Some insight into the concentration fields that underlie these linked and knotted structures can be gained by examining the concentration profiles of

both the activator and inhibitor species. In the colour plate we display the composite picture of the two iso-surface fields: B -field concentration 0.16 and A -field concentration 0.5. The A field is sharp and its iso-surface is insensitive to the exact value of the concentration. From the form of the iso-surface profiles we deduce that the filament repulsion is mediated by the B field and the thickness of the resulting tube is approximately independent of the filament surroundings. A two-dimensional picture of these concentration profiles for a cut through a three-dimensional Borromean ring pattern shown in Fig. 7. One sees the features described above: the A field is very sharp while the B field concentration that couples the fronts is diffuse.

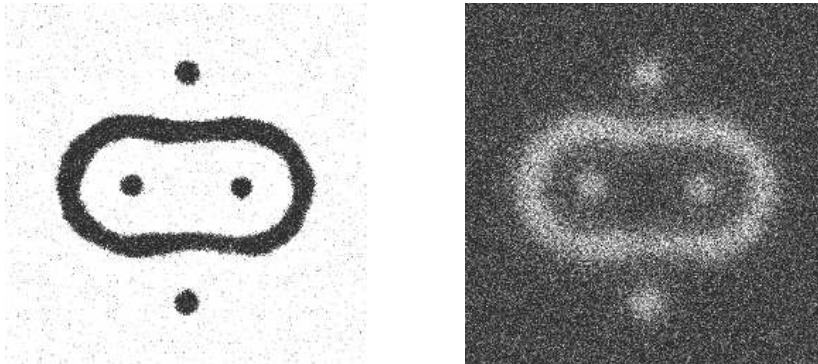


Figure 7: Concentration fields in a two-dimensional cut through the Borromean rings.

We now discuss the ideality of the linked and knotted chemical patterns. An ideal form of a knot or link, constructed from a tube of uniform diameter, has the highest ratio of volume to surface area.⁴ The knotted patterns in the bistable chemical medium appear as iso-surfaces of the concentration fields and can be approximated to a good degree by uniform tubes drawn around closed filaments. Some deviations from ideality are to be expected since we can see that the tubular domains corresponding to the iso-concentration surfaces do not have uniform diameters. However, these deviations are not large and it is interesting to examine the extent to which such ideality applies.

To determine the ideal configurations we extracted the curves $\mathbf{R}(\sigma)$ from the three-dimensional concentration patterns as discussed above. Tubular domains with given radii were then constructed with the curves $\mathbf{R}(\sigma)$ at their centers. The ideal configurations of the 3_1 and 4_1 knots are shown in Fig. 8

Deviations from uniformity of the knotted patterns make it preferable to use integral characteristics of the patterns for the extraction of the system



Figure 8: Approximately ideal representations of the 3_1 and 4_1 knots. A tubular domains of radius 17 are built around the middle line of the patterns.

parameters. The Weyl formula for the volume of the tube in three dimensions relates the volume of the tube to the tube length and diameter:

$$V = \frac{1}{4}\pi D^2 L, \tag{18}$$

where V , D and L are the tube volume, diameter and length, respectively. In Table 1 we compare the computed volume to diameter ratio for two iso-surface concentrations and compare the results with the data for the ideal knots.⁴

Pattern	length(L)	volume $\times 1/64$		L/D		
		(0.13)	(0.16)	(0.13)	(0.16)	ideal
3_1 knot	666	12968	8437	16.7	20.5	16.4
4_1 knot	887	17983	11392	21.8	27.4	21.2
Borromean	427×3	25909	16265	10.5	13.3	
Hopf	264×2	10291	6715	6.6	8.2	6.1

Table 1: Length to diameter ratios for various knots and links.

From this Table we observe that the radii of the tubular domains, determined using Eq. (18) and the measured lengths and volumes, are the same, regardless of the type of link or knot. We find $D \approx 20$ and $D \approx 16$ for the 0.13 and 0.16 iso-concentration surfaces, respectively. This indicates that a consistent tubular representation is possible for all structures. The theoretical radii

of the patterns, computed using the length of the filaments and the theoretical length to diameter ratios^d, are close to those of the 0.13 iso-concentration surface, indicating the ideal character of the observed knots and links.

5 Conclusion

The linked and knotted patterns we have described in this chapter should be observable in experiments on chemical and other systems. Experiments on the iodide-ferrocyanide-sulfite system²¹⁻²³ in quasi two-dimensional geometries have shown the existence of labyrinthine and patterns and localized structures which involve front repulsion for their existence. The main difficulty in finding the three-dimensional topologically stabilized structures is the experimental preparation of the proper initial conditions. Perhaps one way to find such structures is to start from random initial conditions. Since the compact patterns lie in the parameter regime where tubular domains shrink to balls, any structures that are not topologically stabilized will shrink and the structures of interest will survive.

The chemical system we have considered provides an example where the final linked or knotted geometry is the result of the evolution of a nonlinear, dissipative system where there is no free energy functional. The links and knots are compact attracting states of the reaction-diffusion equation (or more specifically the Markov chain dynamics in our stochastic model). In this sense the factors governing the evolution and forms of the patterns are quite different from other cases where potential energy functions have been associated to knots to determine their geometry²⁴ or applications that use the non-dissipative Euler equations of fluid mechanics²⁵ As discussed above, the stable structures arise from the fact that one is in a parameter regime where the tubular domains containing one of the phases shrink, but the geometry of the tubular domain in conjunction with the repulsion between fronts prevents collapse and leads to a stable pattern.

The structures we have described are also quite distinct from the linked and knotted vortex filaments seen in excitable and oscillatory media, even for the same FitzHugh-Nagumo model explored here.^{26,27} The excitable regime corresponds to the case where the system is monostable. The stable fixed point is susceptible to finite amplitude perturbations which lead to large excursions in phase space before return to the fixed point. The singular filaments are the cores of three-dimensional spiral waves. Since our tubular domains are composed of one of the two bistable states and have no phase field associated

^dWe use the value 2π for the Hopf link.

with them that can give rise to twist in the filaments, their structure is actually much simpler than that of vortex filaments.

The fact that the links and knots assume nearly ideal forms seems natural in view of the factors that determine their structure: tubular domain contraction and front repulsion. It would be interesting to explore further the factors that determine the geometries of these stable structures.

Acknowledgments

This work was supported in part by a grant from the Natural Sciences and Engineering Research Council of Canada.

Appendix: System evolution in the Boltzmann approximation

The analysis in Sec. 3 can be made rigorous by analyzing the system in the Boltzmann approximation. In this case the particle distributions at different nodes are considered to be independent so that the state probability distribution is approximated by the product of the reduced 1-node probability distributions:

$$P(\{n_{\mathbf{r}}\}, \{m_{\mathbf{r}}\}, t) = \prod_{\mathbf{r}} p(n, m, \mathbf{r}, t) . \quad (19)$$

The evolution of the node probability distribution is described by the Markov process where the transition matrix is the composition of diffusion and reaction operators:

$$p(n, m, \mathbf{r}, t + 1) = \widehat{\mathbf{W}}^C \widehat{\mathbf{W}}^{D_a}(\bar{a}) \widehat{\mathbf{W}}^{D_b}(\bar{b}) p(n, m, \mathbf{r}, t) . \quad (20)$$

The operators $\widehat{\mathbf{W}}^{D_a}$ and $\widehat{\mathbf{W}}^{D_b}$ are non-local and depend on the states at the surrounding nodes and have the following form:

$$\begin{aligned} W_{n,n'}^{D_{i=(a,b)}}(c) &= \left[1 - \bar{c} \left(1 - \frac{n'}{N} \right) + (1 - \bar{c}) \frac{n'}{N} \right] \delta_{n',n} \\ &\quad + \bar{c} \left(1 - \frac{n'}{N} \right) \delta_{n',n-1} + (1 - \bar{c}) \frac{n'}{N} \delta_{n',n+1} , \end{aligned} \quad (21)$$

where \bar{c} is the average particle density of the neighbouring sites:

$$\bar{c}(\mathbf{r}, t) N = \frac{1}{2d} \sum_{\mathbf{r}' \in \mathcal{N}(\mathbf{r})} \sum_n n p(n, m, \mathbf{r}', t) = \frac{1}{2d} \sum_{\mathbf{r}' \in \mathcal{N}(\mathbf{r})} \langle n \rangle(\mathbf{r}', t) . \quad (22)$$

We seek a solution of Eq. (20) in the following form:

$$p(n, m, \mathbf{r}, t) = \sum_{s=0}^{\infty} \varepsilon^s p_s(n, m, a(\mathbf{r}, t), b(\mathbf{r}, t)) , \quad (23)$$

with an additional constraint: $\langle \{n, m\} \rangle_p = N\{a(\mathbf{r}, t), b(\mathbf{r}, t)\}$ for any partial sum. We expand the evolution operator in a series of powers of the ordering parameter:

$$\partial_t = \sum_{s=0}^{\infty} \varepsilon^s \mathcal{D}_s . \quad (24)$$

and rewrite the diffusion and collision operators as:

$$\widehat{\mathbf{W}}^{D_a}(\bar{c}(\mathbf{r}, t)) = \widehat{\mathbf{W}}^{D_a}(a(\mathbf{r}, t)) + \varepsilon \left[\widehat{\mathbf{W}}^{D_a}(\bar{c}(\mathbf{r}, t)) - \widehat{\mathbf{W}}^{D_a}(a(\mathbf{r}, t)) \right] \quad (25)$$

$$\widehat{\mathbf{W}}^C = \mathbf{1} + \varepsilon \widehat{\mathbf{C}} . \quad (26)$$

Following the standard Chapman-Enskog procedure²⁸ we arrive at the following equations at the zeroth and first orders:

$$\widehat{\mathbf{W}}^{D_a} \widehat{\mathbf{W}}^{D_b} p_0(\cdot, \cdot, \mathbf{r}, t) = p_0(\cdot, \cdot, \mathbf{r}, t) \quad (27)$$

$$\mathcal{D}_0 p_0(\cdot, \cdot, \mathbf{r}, t) = \left[\widehat{\mathbf{D}}^b + \widehat{\mathbf{D}}^b + \widehat{\mathbf{C}} \right] p_0(\cdot, \cdot, \mathbf{r}, t) + \widehat{\mathbf{W}}^{D_a} \widehat{\mathbf{W}}^{D_b} p_1(\cdot, \cdot, \mathbf{r}, t) \quad (28)$$

where we denoted the difference in Eq. (25) by $\widehat{\mathbf{D}}^{i=(a,b)}$ and used the invariance of $p_0(\mathbf{r}, t)$ under the action of the commuting operators $\widehat{\mathbf{W}}^{D_a}$ and $\widehat{\mathbf{W}}^{D_b}$.

The stationary probability distribution of (27) is binomial. To show this it is convenient to consider the generating function¹⁷ of the distribution

$$f_s(x, y, \mathbf{r}, t) = \sum_{n,m=0}^N x^n y^m p_s(n, m, a(\mathbf{r}, t), b(\mathbf{r}, t)) . \quad (29)$$

In the generating function representation the diffusion operator takes the form:

$$\widehat{\mathbf{W}}^{D_a}(a) = [1 - a(1 - x)] \left(\mathbf{1} + \frac{1 - x}{N} \partial_x \right) \quad (30)$$

and the particle number expectation value is given by:

$$\langle \{n, m\} \rangle_{p_s} = \left. \left\{ \partial_x f_s(x, y), \partial_y f_s(x, y) \right\} \right|_{x,y=1} . \quad (31)$$

From the above equation we obtain the evolution equation for the particle number expectation under the action of operator $\widehat{\mathbf{W}}^{D_a}(a)$:

$$\langle n \rangle_{\widehat{\mathbf{W}}^{D_a}(a)_p} = af(1, 1) + \frac{N-1}{N} \partial_x f_s(x, y) \Big|_{x, y=1} = a + \frac{N-1}{N} \langle n \rangle_p, \quad (32)$$

and, at equilibrium:

$$\langle n \rangle_{\widehat{\mathbf{D}}^a(a)_{p_0}(\mathbf{r}, t)} = \bar{c}(\mathbf{r}, t) - \frac{1}{N} \langle n \rangle_{p_0(\mathbf{r}, t)} = \frac{1}{2dN} \Delta \langle n \rangle_{p_0(\mathbf{r}, t)} + o(\nabla^3) \quad (33)$$

The eigenvalues of the operator (30) are $\{1 - k/N : k = 0, \dots, N\}$ and the corresponding eigenfunctions are:

$$\phi_k(x) = (1 - a(1 - x))^{N-k} (1 - x)^k, \quad (34)$$

so that the zeroth order approximation is given by a local binomial distribution.

The collision operator in the generating function representation has the following form:

$$\begin{aligned} \widehat{\mathbf{C}} &= \tilde{k}_1(1-x)x^{N+1}\partial_x \frac{1}{x^{N-2}}\partial_{xx} + \tilde{k}_1^*(1-x)x^N\partial_{xx} \frac{1}{x^{N-2}}\partial_x \\ &+ \tilde{k}_2(1-x)x^{N+1}y\partial_{xy} \frac{1}{x^N} - \tilde{k}_2^*(1-x)y^{N+1}\partial_{xy} \frac{1}{y^N} \\ &+ \tilde{k}_3^*(1-y)x\partial_{xy} - \tilde{k}_3(1-y)(xy)^{N+1}\partial_{xy} \frac{1}{y^N x^N}, \end{aligned} \quad (35)$$

where \tilde{k}_i and \tilde{k}_i^* are the reaction rates. Acting with the operators in (31) on equation (28) and approximating the spatial average by the Laplace operator we arrive at the FitzHugh-Nagumo system of equations (1). The reaction rates \tilde{k}_i and \tilde{k}_i^* are proportional to the probabilities of transitions p_j of Eq. (13). Computations yield the following relations between the mass action and the lattice gas kinetics coefficients:

$$k_1 = \frac{N!}{N^3(N-3)!} \tilde{k}_1 \text{ and } k_{2,3} = \tilde{k}_{2,3}. \quad (36)$$

References

1. R. Kapral and K. Showalter, editors. *Chemical Waves and Patterns*. Kluwer, Dordrecht, 1995.
2. A. Malevanets and R. Kapral. Microscopic model for FitzHugh-Nagumo dynamics. *Phys. Rev. E*, 55:5657–5670, 1997.

3. A. Malevanets and R. Kapral. Links, knots, and knotted labyrinths in bistable systems. *Phys. Rev. Lett.*, 77:767–771, 1996.
4. V. Katritch, J. Bednar, D. Michoud, R.G. Scharein, J. Dubochet, and A. Stasiak. Geometry and physics of knots. *Nature*, 384:142–145, 1996.
5. R. FitzHugh. Impulses and physiological states in theoretical models of nerve membrane. *Biophysical Journal*, 1:445–466, 1961.
6. J. S. Nagumo, S. Arimoto, and Y. Yoshikawa. *Proc. IRE*, 50(2061), 1962.
7. P. C. Hohenberg and B. I. Halperin. Theory of dynamical critical phenomena. *Rev. Mod. Phys.*, 49(435), 1977.
8. J. D. Gunton and M. Droz. *Introduction to the theory of metastable and unstable states*, vol. 183 of *Lecture notes in physics*. Springer-Verlag, New York, 1983.
9. T. Ohta and R. Mimura, M. Kobayashi. Higher-dimensional localized patterns in excitable media. *Physica D*, 34:115–144, 1989.
10. T. Ohta, A. Ito, and A. Tetsuka. Self-organization in an excitable reaction-diffusion systems. *Phys. Rev. A*, 42:3225–3233, 1990.
11. D. M. Petrich and R. E. Goldstein, Nonlocal contour dynamics model for chemical front motion. *Phys. Rev. Lett.* 72: 1120–1123, 1994.
12. R. E. Goldstein, D. J. Muraki and D. M. Petrich, Interface proliferation and the growth of labyrinths in a reaction-diffusion system. *Phys. Rev. E*, 53: 3933–3957, 1996.
13. A. Hagberg and E. Meron. Domain walls in nonequilibrium systems and emergence of persistent patterns. *Phys. Rev. E.*, 49:5046–5057, 1994.
14. A. Hagberg and E. Meron. From labyrinthine patterns to spiral turbulence. *Phys. Rev. Lett.*, 72:2494–2497, 1994.
15. K. A. Gorshkov, A. S. Lomov, and M. I. Rabinovich. 3-dimensional particle-like solutions of coupled nonlinear fields. *Phys. Lett. A*, 137:250–254, 1989.
16. I. S. Aranson, K. A. Gorshkov, A. S. Lomov, and M. I. Rabinovich. Stable particle-like solutions of multidimensional nonlinear fields. *Physica D*, 43:435–453, 1990.
17. C. W. Gardiner. *Handbook of Stochastic Methods*, vol. 13 of *Springer Series in Synergetics*. Springer-Verlag, Berlin, 2 edition, 1985.
18. U. Frisch, D. d’Humières, B. Hasslacher, P. Lallemand, Y. Pomeau, and J.-P. Rivet. Lattice gas hydrodynamics in two and three dimensions. *Complex Systems*, 1:649–707, 1987.
19. N. Margolus. CAM-8: A computer architecture based on cellular automata. In R. Kapral and A. Lawniczak, editors, *Pattern Formation and Lattice-Gas Automata*, p. 165. Fields Institute Communications,

- AMS, 1996.
20. B. A. Dubrovin, A. T. Fomenko, and S. P. Novikov. *Modern geometry—methods and applications*, vol. 93 of *Graduate texts in mathematics*. Springer-Verlag, New York, 2nd edition, 1992.
 21. K. J. Lee and H. L. Swinney. Lamellar structures and self-replicating spots in a reaction-diffusion system. *Phys. Rev. E*, 51:1899–1915, 1995.
 22. K. J. Lee, W. D. McCormick, J. E. Pearson, and H. L. Swinney. Experimental observation of self-replicating spots in a reaction-diffusion system. *Nature*, 369:215–218, 1994.
 23. K. J. Lee, W. D. McCormick, Q. Ouyang, and H. L. Swinney. Pattern-formation by interacting chemical fronts. *Science*, 261:192–194, 1993.
 24. G. Buck and J. Simon. Knots as dynamical-systems. *Topology and its applications*, 51:229–246, 1993.
 25. H. K. Moffat. The energy spectrum of knots and links. *Nature*, 347:367–369, 1990.
 26. A. T. Winfree. Stable particle-like solutions to the nonlinear wave equations of the three-dimensional excitable media. *SIAM Review*, 32:1–53, 1990.
 27. M. Courtemanche, W. Skaggs, and A. T. Winfree. Stable 3-dimensional action-potential circulation in the FitzHugh-Nagumo model. *Physica D*, 41:173–182, 1990.
 28. S. Chapman and T. G. Cowling. *Mathematical Theory of Non-Uniform Gases*. Cambridge University Press, Cambridge, 1952.